Universal scaling behavior under pressure in the heavy-fermion antiferromagnet $CeRh_2Si_2$: ^{29}Si NMR study

H. Sakai,* Y. Matsumoto,† Y. Haga, Y. Tokunaga, and S. Kambe
Advanced Science Research Center, Japan Atomic Energy Agency, Tokai, Ibaraki 319-1195, Japan

(Received 10 November 2020; revised 7 January 2021; accepted 28 January 2021; published 10 February 2021)

The microscopic origin of a magnetic phase diagram under pressure in the heavy-fermion antiferromagnet $CeRh_2Si_2$ was investigated using the ^{29}Si nuclear magnetic resonance (NMR) technique. Owing to the characteristics of the hyperfine form factor at the Si site, which filters specific $\boldsymbol{q}$-dependent fluctuations around antiferromagnetic $\boldsymbol{q}$ vectors, we investigated the temperature and pressure dependences of $\boldsymbol{q}$-independent local fluctuations caused by the single-site Kondo effect. A universal scaling behavior observed on the energy scale of the local fluctuations in the entire pressure region demonstrates that the characteristic energy scale T_0 of Kondo interactions monotonically increases by applying pressure without a critical anomaly around the quantum critical pressure P_c of antiferromagnetism. Our NMR result agrees with the Doniach picture of the heavy-fermion phase diagram, where the progressive delocalization of the f electrons occurs across P_c, accompanied by the development of antiferromagnetic correlations among the f electrons.

DOI: 10.1103/PhysRevB.103.085114

I. INTRODUCTION

In strongly correlated f-electron systems, various intriguing phases are found near the quantum critical transition, which arises because of competitive and/or cooperative interactions within a small energy scale. The case of an antiferromagnetic (AFM) heavy fermion (HF) is considered as a standard example, yielding the so-called Doniach picture [1], to realize a quantum phase transition between AFM and paramagnetic (PM) states via chemical doping or by applying pressure or magnetic field. Kondo interactions drive the formation of Kondo singlets between the local moments and conduction electrons. At high temperatures, the system is in a fully incoherent regime with local moments. As the temperature decreases below T_K, which is the energy scale of Kondo interactions, the local moments are gradually screened and counted in the Fermi volume. Alternatively, the intersite AFM Ruderman-Kittel-Kasuya-Yosida interactions promote the singlet formations among the local moments and develop the AFM order, thereby competing with the Kondo interactions.

In the prototypical AFM HF compounds $CeCu_6$ and $CeRu_2Si_2$, inelastic neutron scattering experiments have revealed that the local $\boldsymbol{q}$-independent fluctuations caused by the single-site Kondo interactions coexist with the $\boldsymbol{q}$-dependent fluctuations induced by the intersite AFM correlations [2]. Similarly, in the chemical doping system of the AFM HF $Ce_{1-x}La_xRu_2Si_2$, the $\boldsymbol{q}$-dependent and $\boldsymbol{q}$-independent fluctuations have been evaluated separately [3]. By increasing the x of La doping, the energy scale $\Gamma_{\boldsymbol{Q}}$ of AFM spin fluctuations (SFs) sharply decreases and becomes nearly zero at the critical composition of $x_c \approx 0.075$, and it increases above x_c, following the T_N tendency. Alternatively, the energy scale Γ_0 of local fluctuations induced by Kondo interactions monotonically decreases all the way until it reaches zero without a critical anomaly at x_c. Thus, in this AFM HF system, the AFM SFs are considered the driving force for the quantum critical transition at x_c. Conversely, in the local quantum criticality framework [4,5], the Kondo singlet is critically destroyed at the quantum critical point where the AFM transition occurs at $T = 0$, along with a sudden change in the localized itinerant f character. In such a case, Γ_0 as well as $\Gamma_{\boldsymbol{Q}}$ should be sharply reduced at the critical point. Therefore, to examine the quantum criticality in a subjective AFM HF material, it is important to estimate $\Gamma_{\boldsymbol{Q}}$ and Γ_0 separately. However, in many AFM HF cases it is difficult to separately measure the local fluctuations because AFM SFs are markedly enhanced in the foreground.

The HF antiferromagnet $CeRh_2Si_2$ exhibits successive AFM orderings at $T_{N1} = 36$ K and $T_{N2} = 25$ K [6–9]. When a pressure of approximately $P_c \simeq 1$ GPa is applied, the AFM transition is completely suppressed, and superconductivity is induced at a temperature below 0.4 K [10–12]. Simultaneously, a sudden change in the Fermi surfaces occurs at P_c, which is detected using the de Haas–van Alphen effect [13] and thermoelectric power [14] measurements. Moreover, a discontinuity of lattice volume at P_c is detected using thermal expansion measurements [15]. Because of such discontinuous changes, the importance of valence fluctuations is suggested [14]. Therefore, it is particularly crucial to examine the development of local fluctuations induced by Kondo interactions under pressure. In the PM state, the static susceptibility shows strong uniaxial anisotropy along the c axis. Its crystal electrical field (CEF) ground state is a doublet $\Gamma_7^{(1)}$, and the

*sakai.hironori@jaea.go.jp
†Present address: Graduate School of Science and Engineering, University of Toyama, Toyama 930-8555, Japan.

first excited level of the next doublet $\Gamma_7^{(2)}$ is greater than ∼300 K [8]. This CEF level scheme was confirmed using x-ray absorption spectroscopy and inelastic neutron scattering measurements [16,17]. Thus, CEF excitation is unrelated to the lowest-lying excitations in this system.

The nuclear magnetic resonance (NMR) technique is a powerful tool for detecting AFM SFs at a specific $\boldsymbol{Q}$. However, in this study, an incidental characteristic of the hyperfine form factor of the ^{29}Si NMR in $CeRh_2Si_2$ enables us to extract the temperature and pressure dependences of $\boldsymbol{q}$-independent local fluctuations caused by the single-site Kondo effect. The use of hydrostatic pressure as a tuning parameter can avoid the introduction of any randomness effect, other than chemical substitution/alloying. The remainder of this study is presented as follows. In Sec. II, experimental details are provided. In Sec. III A, we report the static magnetism and hyperfine coupling constants for ^{29}Si of $CeRh_2Si_2$ under pressure. In Sec. III B, we show the results of the NMR relaxation rates $(1/T_1)$ obtained under pressure and discuss the dynamical aspect of the electronic properties in the PM state. In Sec. III C, we observe the characteristic energy scale of the local fluctuations caused by the Kondo interactions in this compound. Finally, a summary of the NMR study is presented in Sec. IV.

II. EXPERIMENT

Single crystals of $CeRh_2Si_2$ were grown using the Czochralski method. The starting materials were Ce, Rh, natural Si, and 99.3% ^{29}Si-enriched Si. The ^{29}Si nuclei with a nuclear spin of $I = \frac{1}{2}$ have a relatively large gyromagnetic ratio $\gamma_n = 0.84577$ MHz/kOe; however, the natural abundance of ^{29}Si is only 4.7%. To increase NMR sensitivity, the isotopic density of ^{29}Si was enriched up to 50% in the $CeRh_2Si_2$ crystals. The single phase was confirmed using x-ray diffraction, electron probe microanalysis, and magnetization measurements.

NMR measurements were performed in the temperature range of 1.5–300 K using a phase-coherent, pulsed spectrometer. Frequency-swept spectra at a constant field were obtained with the radio frequency (r.f.) network tuned and matched at each point. To form nuclear spin echoes, 90°−180° conditions were used with a first-pulse duration of 2–3 μs, where the r.f. power for nuclear spin excitation was optimized at each NMR spectral peak. The separation τ between the first and second pulses was typically 10–30 μs. Each spin echo signal was accumulated and subjected to fast Fourier transform.

For NMR measurements at ambient pressure, external fields were calibrated using the NMR frequencies of ^{63}Cu in an NMR coil and ^{195}Pt in platinum powder inserted as the field marker. To apply hydrostatic pressures, a standard hybrid piston-cylinder-type clamp cell was used with Daphne 7373 lubricant oil (Idemitsu Kosan Co. Ltd., Tokyo, Japan) as the pressure medium. Two single crystals with dimensions of $\sim 1 \times 2 \times 0.5$ mm^3 and a powder of cuprous oxide (Cu_2O) were inserted into three separate NMR pickup coils composed of Cu metal. One crystal was set with the condition of $H_0 \parallel c$, and another was set with that of $H_0 \parallel a$ in the pressure cell. The orientations of the single crystals were double-checked by comparing the NMR shift values measured inside and outside of the cell at ambient pressure ($P = 0$ GPa). The nuclear quadrupole resonance (NQR) frequency of the ^{63}Cu nuclei in Cu_2O was used as the measure of pressure, and the NMR shift of Cu metal was used to determine the external field in the cell [18].

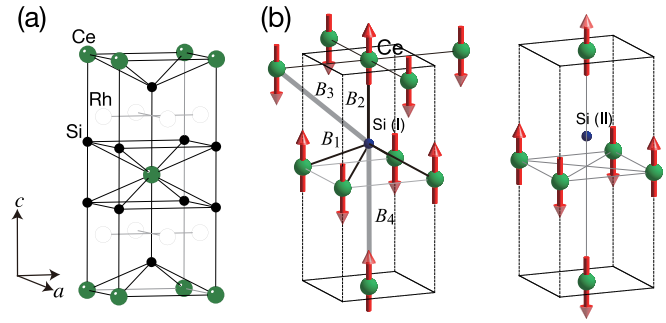

FIG. 1. (a) Crystal structure of $CeRh_2Si_2$. (b) Two types of local environments of the Si sites in the 4$\boldsymbol{q}$-magnetic structure, where the Rh atoms are excluded for simplicity.

The inversion recovery method was used to determine $1/T_1$. The $1/T_1$ values were deduced from the recovery curve of nuclear magnetization by fitting to the single-exponential function $\{M_n(\infty) - M(t)\}/M(\infty) \propto \exp(-t/T_1)$ for nuclear spin $I = 1/2$.

III. RESULTS AND DISCUSSION

A. Static magnetism and NMR shifts

$CeRh_2Si_2$ crystalizes in a tetragonal $ThCr_2Si_2$-type structure [Fig. 1(a)]. The anisotropy of magnetic susceptibility is very large in $CeRh_2Si_2$ at the ambient pressure; the magnetic susceptibility $\chi_c(0)$ in the c direction is considerably larger than χ_a in the a direction [8]. Both $\chi_c(0)$ and $\chi_a(0)$ appear to follow the Curie-Weiss law above ∼100 K. As the temperature decreases, $\chi_c(0)$ shows a broad maximum at approximately T^*, which is slightly above $T_{N1} = 36$ K. Then, $\chi_c(0)$ rapidly decreases just below T_{N1} and shows no clear anomaly at $T_{N2} = 25$ K. The $\chi_i(0)$ data ($i = c$ and a) of the ^{29}Si enriched crystal are entirely consistent with the previous result [8]. In the lowest-temperature region well below T_{N1} and T_{N2}, our crystal does not show any Curie-like upturn, indicating that our crystal is free from any magnetic impurities.

The pressure variations for $\chi_i(0)$ ($i = c$ and a) in $CeRh_2Si_2$ were previously reported by two independent research groups: one by Muramatsu *et al.* [19] and the other by Mori *et al.* [20]. The former group [19] reported that the magnetic susceptibility $\chi_c(0)$ for $H_0 \parallel c$ is gradually suppressed by applying pressures of up to $P \simeq 1.3$ GPa and that the temperature dependence of $\chi_c(0)$ exhibits a broad maximum at approximately $T^* \simeq 70$ K under $P \simeq 1.3$ GPa. Alternatively, in the report by the latter group [20], T^* did not shift by applying pressures of up to 1 GPa, while the values of $\chi_c(0)$ were moderately suppressed. Furthermore, the former group [19] reported that the $\chi_a(0)$ values decreased when applying pressure; however, the latter group [20] observed that these values increased. As shown in Figs. 2(a) and 2(b), T^* values for both the c and a axes increased, and the NMR shifts in the case of $H_0 \parallel a$ decreased when applying pressure. Therefore, the $\chi_i(0)$ data under pressure by the former group [19] are

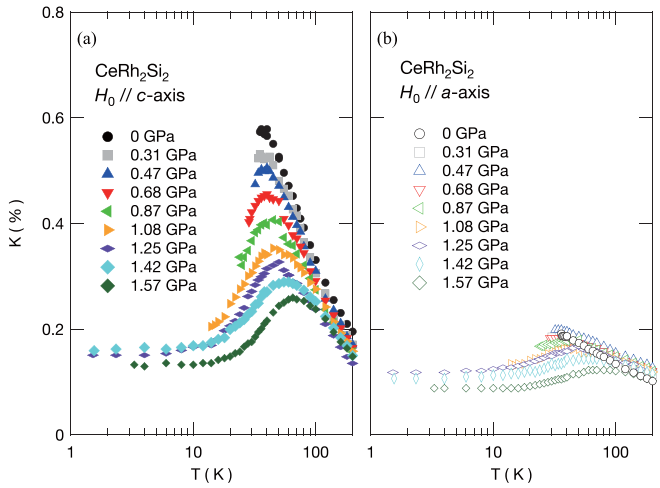

FIG. 2. Temperature dependence of ^{29}Si NMR shifts in $CeRh_2Si_2$ under various applied pressures for (a) $H_0 \parallel c$ and (b) $H_0 \parallel a$.

adopted later to deduce the hyperfine coupling constant A_i in the i direction.

Figure 3 shows ^{29}Si NMR spectra at 40 K (PM state), 30 K (below T_{N1}), and 4.5 K (below T_{N2}) measured at a constant field of $H_0 \sim 72.1$ kOe along the c and a axes. In the case of $H_0 \parallel c$, the ^{29}Si-NMR spectrum with $I = \frac{1}{2}$ is a single line in the PM state; then, it splits into two lines below T_{N1} and becomes four lines below T_{N2}, where the center of gravity shifts to the lower-frequency side when the temperature is decreased below T_{N1}. This observation is consistent with a previous NMR result using powder aligned to the c axis [21]. In the case of $H_0 \parallel a$, the sharper spectrum remains as a single line below T_{N1} and T_{N2}, and the spectral position does not shift considerably.

In the PM state, the respective NMR peak frequency ν_{res} determines the value of the NMR shift, i.e.,

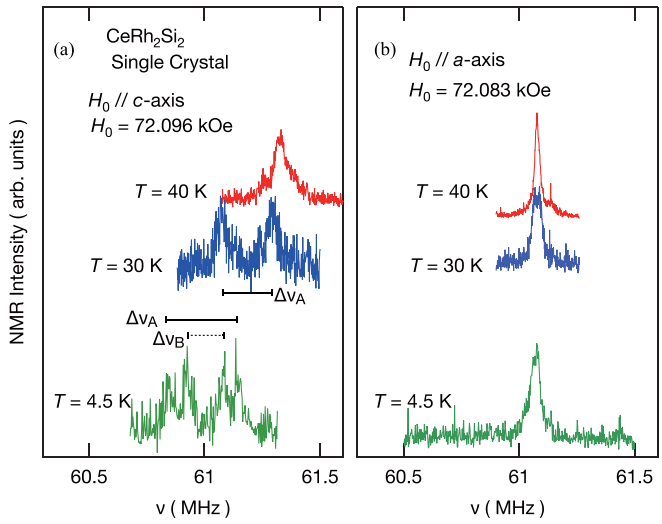

FIG. 3. ^{29}Si NMR spectra of a single crystal of $CeRh_2Si_2$ enriched with 50% ^{29}Si at a constant field of $H_0 \sim 72.1$ kOe along (a) the c axis and (b) a axis at temperatures of 40 K (above T_{N1}), 30 K (below T_{N1}), and 4.5 K (below T_{N2}).

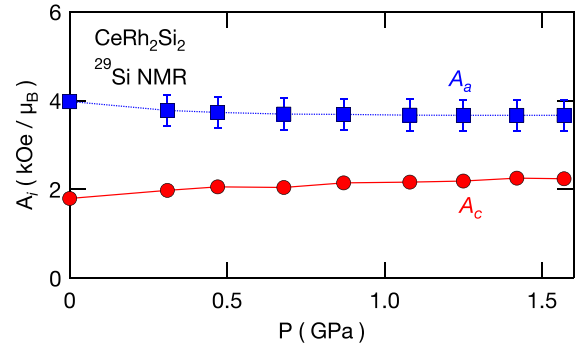

FIG. 4. Pressure dependence of transferred hyperfine coupling constants A_i ($i = c$ and a) for ^{29}Si in $CeRh_2Si_2$.

$K \equiv \{\nu_{res} - \gamma_n H_0\}/\gamma_n H_0$. The NMR shifts K_c and K_a in the c and a axes increase as the temperature decreases in the PM state (Fig. 2), where the temperature dependence is similar to that in static susceptibility $\chi_i(0)$. The anisotropy of K is also similar to that in $\chi_i(0)$. The hyperfine coupling constants A_c and A_a in the c and a directions are derived as 1.84 ± 0.01 and 3.98 ± 0.04 kOe/μ_B, respectively [22], from the so-called K-χ plots with temperatures as an implicit parameter. The transferred hyperfine coupling constants $A_i \equiv K/\chi_i(0)$ under pressures are plotted in Fig. 4. Here, $\chi_i(0)$ data [19] under pressure are interpolated and extrapolated at each pressure below and above ~1 GPa, respectively. Both A_c and A_a vary very slightly with the application of pressure (Fig. 4).

In the AFM state [Fig. 3(a)], the two frequency widths $\Delta\nu_A$ and $\Delta\nu_B$ well below T_{N2} correspond to internal fields $H_{int}(A)$ and $H_{int}(B)$, respectively. In other words, the four NMR lines arise from the resonant fields of $H_0 \pm H_{int}(A)$ and $H_0 \pm H_{int}(B)$ in the AFM arrangement of Ce moments. In the AFM state between T_{N1} and T_{N2}, all the Si sites are equivalent, so that the NMR occurs with $H_0 \pm H_{int}(A)$. The values of $H_{int}(A)$ and $H_{int}(B)$ at $T \to 0$ are obtained as 0.177 and 0.092 kOe, respectively. In the case of $H_0 \parallel a$, no a projection of internal fields is observed, indicating that each Ce moment is an *Ising*-type moment (up and down) in the AFM ordered state.

As shown in Fig. 1(b), the transferred hyperfine fields $H_{int}(A, B)$ in the AFM state are caused not by the first-nearest-neighbor (NN) Ce ions, but by the second-, third-, and, at least fourth-NN Ce ions. As noted by Kawarazaki *et al.* [23], two magnetically inequivalent Si sites will appear in the $4\boldsymbol{q}$ structure below T_{N2}. Because the first-NN hyperfine fields are fully canceled on the Si sites in the AFM arrangement with $\boldsymbol{Q}_1 = (1/2, 1/2, 0)$ and/or $\boldsymbol{Q}_2 = (1/2, 1/2, 1/2)$, the two different internal fields observed should arise from the second-, third-, fourth-, or farther-NN Ce ions. As discussed in Ref. [22], as a minimum model to describe the transferred hyperfine fields on the Si sites, at least fourth-NN Ce ions must be considered, i.e., $A_c = 4B_1 + B_2 + 4B_3 + B_4$ in the PM state. Then, in the AFM state, the hyperfine fields are transferred as $\pm|(B_2 - 4B_3)|\mu_{ord}$ below T_{N1} and $[\pm|(B_2 - 4B_3)| \pm |B_4|]\mu_{ord}$ below T_{N2}. Assume that $B_j \propto 1/r_j^3$, where r_j is the distance from the magnetic ion; then B_j ($j = 1, 2, 3, 4$) is estimated as 0.37, 0.12, 0.037, and 0.098 kOe/μ_B, respectively. As noted in Sec. III B, these hyperfine coupling constants B_j are helpful to discuss how the hyperfine form factor filters the AFM SFs from $1/T_1$.

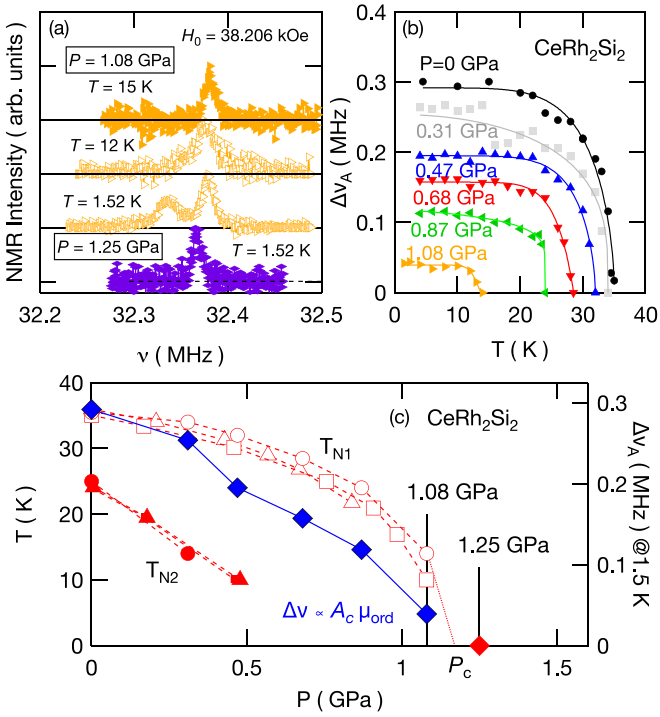

FIG. 5. (a) ^{29}Si NMR spectra with an external field of $H_0 =$ 38.2 kOe at $T = 15$, 12, and 1.52 K under $P = 1.08$ GPa and at $T = 1.52$ K under $P = 1.25$ GPa. (b) Temperature dependence of the NMR line split $\Delta\nu_A$ under various pressures. The solid curves are drawn to guide the eyes. (c) T-P phase diagram for $CeRh_2Si_2$. The open and solid circles represent T_{N1} and T_{N2} determined using the NMR experiment. The pressure dependence of the NMR line split $\Delta\nu_A$ at 1.5 K is also plotted. The AFM transition temperatures of T_{N1} and T_{N2} (open and solid squares) determined using neutron diffraction in Ref. [23] and resistivity (open and solid triangles) in Ref. [12] are also plotted.

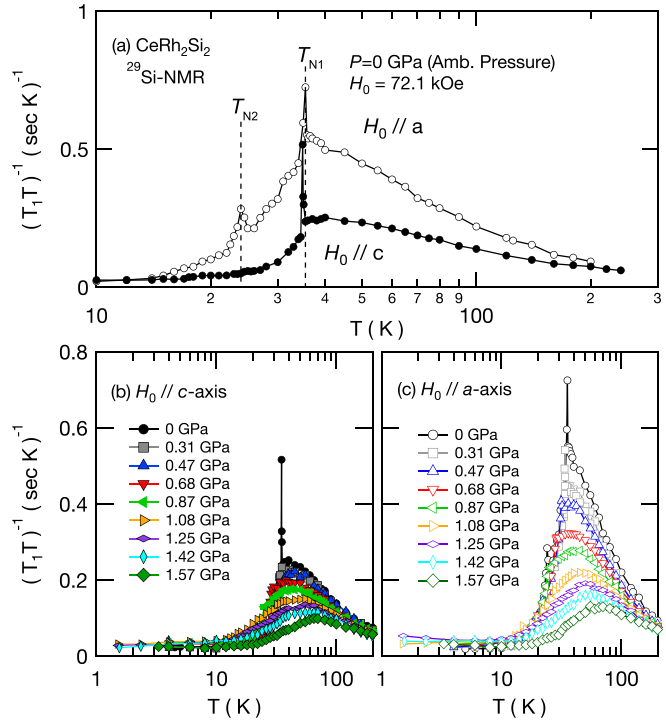

FIG. 6. (a) Temperature dependence of $(T_1T)^{-1}$ for ^{29}Si NMR in $CeRh_2Si_2$ at ambient pressure when applying an external field of 72.1 kOe parallel to the respective crystallographic axis of c and a. Pressure variations of $(T_1T)^{-1}$ in the PM state are shown for (b) $H_0 \parallel c$ and (c) $H_0 \parallel a$.

To specify the exact critical pressure P_c of the AFM state, ^{29}Si NMR spectra at $P = 1.08$ and 1.25 GPa are shown in Fig. 5(a). At $P = 1.08$ GPa [Figs. 5(a) and 5(b)], the NMR line is broadened below $T_{N1}(P) = 14$ K, and the line clearly splits at 1.52 K. $T_{N1}(P)$ is approximately consistent with the findings obtained from neutron scattering [23] [Fig. 5(c)]. However, for an applied pressure of 1.25 GPa, the NMR line splitting is not observed at 1.52 K. As plotted in Fig. 5(c), the split frequency $\Delta\nu_A$, which is proportional to $A_c\mu_{ord}$, approaches zero at P_c. From the current NMR study, P_c can be estimated to lie between 1.08 and 1.25 GPa because T_{N1} and $\Delta\nu_A$ approach zero in this area [Fig. 5(c)]. An indication of superconductivity is reported in the pressure region of 0.97–1.20 GPa using a high-purity single crystal [12]. Note that zero resistivity is realized in an extremely narrow pressure region of 1.03–1.08 GPa.

B. NMR relaxation rates and dynamical magnetic responses

Figure 6(a) shows the $(T_1T)^{-1}$ vs T plots for ^{29}Si NMR in $CeRh_2Si_2$ when applying fields along the c and a axes at ambient pressure. The anisotropy in $(T_1T)^{-1}$ is opposite that in K; $(T_1T)^{-1}_{H_0\parallel a}$ is larger than $(T_1T)^{-1}_{H_0\parallel c}$. In the PM state, as the temperature decreases from 250 K, the $(T_1T)^{-1}$ values in both directions increase with the Curie-Weiss-like T dependence. The $(T_1T)^{-1}$ value seems to saturate slightly above T_{N1} and shows a critical slowing down in a narrow temperature region just above T_{N1}. Then, $(T_1T)^{-1}$ sharply decreases below T_{N1}. At T_{N2}, $(T_1T)^{-1}_{H_0\parallel a}$ shows a critical slowing down again, while $(T_1T)^{-1}_{H_0\parallel c}$ has no anomaly at T_{N2}.

The pressure variations of the $(T_1T)^{-1}$ vs T plots in the PM state in the cases of $H_0 \parallel c$ and $H_0 \parallel a$ are shown in Figs. 6(b) and 6(c), respectively. Although the sharp critical peaks of $(T_1T)^{-1}$ at T_{N1} and T_{N2} would fade due to the small pressure distribution, T_{N1} can be tracked by the sudden decrease in $(T_1T)^{-1}$ and the occurrence of the NMR spectral split shown in Fig. 3. When applying P, T_{N1} shifts to the lower-temperature side and disappears between 1.08 and 1.25 GPa, as already described in Sec. III A. The broad hump structure of $(T_1T)^{-1}$ remains at approximately T^*, although T^* shifts to the higher-temperature side, as observed in the K data in Fig. 2(a).

T^* gradually increases from 36 K ($P = 0$ GPa) to 65 K ($P = 1.57$ GPa) with an increase in P. Interestingly, the Hall resistance $R_H(P)$, which may be related to staggered susceptibility $\chi(\boldsymbol{Q})$ [24], exhibits similar maxima at $T^*(P)$ in the $R_H(P)$-T plot [25]. In magnetoresistance measurements [26], T^* has been regarded as an AFM correlation energy.

Generally, $1/T_1$ in units of $k_B = \hbar = 1$ can be expressed [27] as

$$\frac{1}{T_1} = 2T(\gamma_n A_\perp)^2 \sum_{\boldsymbol{q}} f^2(\boldsymbol{q}) \frac{\mathrm{Im}\chi_\perp(\boldsymbol{q},\omega_0)}{\omega_0}, \qquad (1)$$

where $f(\boldsymbol{q})$ is the hyperfine form factor (considered to be unity for simplicity in most cases), $\mathrm{Im}\chi(\boldsymbol{q},\omega_0)$ is the imaginary part of the dynamical susceptibility, ω_0 is the nuclear Larmor frequency, and $\perp$ refers to the component perpendicular to the quantization axis. Thus, $(T_1T)^{-1}$ corresponds to perpendicular SFs in an applied external field.

$f(\boldsymbol{q})$ can be expressed using such a geometrical configuration of the Si sites:

$$f(\boldsymbol{q}) \approx |A|^{-1}\{B_1(e^{i[q_x+q_y-q_z(1-2z)]/2}+\cdots) + B_2e^{\mathrm{i}zq_z} + B_3(\cdots) + B_4e^{\mathrm{i}(1-z)q_z}\}, \quad (2)$$

where $z = 0.3737$ is a positional parameter for Si sites in the crystal structure, as shown in Fig. 1(a). At specific AFM propagation vectors $q_x = \pi$ and/or $q_y = \pi$, $F(\boldsymbol{q}) \equiv f^2(\boldsymbol{q})$ becomes zero; however, it gradually approaches zero from the adjacent $\boldsymbol{q}$ positions because the $\boldsymbol{q}$ dependence of $F(\boldsymbol{q})$ is a trigonometric function. Usually, $(T_1T)^{-1}$ can detect AFM SFs even if $F(\boldsymbol{q})$ may lessen the element of $F(\boldsymbol{q})\mathrm{Im}\chi(\boldsymbol{q},\omega_0)$ around the specific $\boldsymbol{Q}$'s in Eq. (1) because $\mathrm{Im}\chi(\boldsymbol{q},\omega_0)$ in normal metals has a broad width in the $\boldsymbol{q}$ space. However, if $\mathrm{Im}\chi(\boldsymbol{q},\omega_0)$ has a sharp $\boldsymbol{q}$ dependence and/or if $F(\boldsymbol{q})$ considerably filter the specific $\boldsymbol{Q}$ fluctuations, $(T_1T)^{-1}$ can no longer detect such specific AFM SFs.

In the PM state of $CeRh_2Si_2$, AFM SFs are enhanced at $\boldsymbol{Q}_1$ and/or $\boldsymbol{Q}_2$; thus, the AFM critical slowing down is observed at T_{N1} (and at T_{N2}) in Fig. 6(a), although the AFM SFs are severely filtered because of $F(\boldsymbol{Q}_1)$ or $F(\boldsymbol{Q}_2) \approx (B_2 - 4B_3)^2/A_c^2 \approx 2\times10^{-4}$. This would be the reason why the T window showing the AFM critical slowing down is very narrow. In such a case, the overall $(T_1T)^{-1}$, except for the critical slowing down region, represents the $\boldsymbol{q}$-independent dynamical response filtered by $F(\boldsymbol{q})$ in the Si sites and the specific AFM SFs in $CeRh_2Si_2$. In other words, the geometrical factor is not necessarily needed to interpret $(T_1T)^{-1}$ in the PM state of $CeRh_2Si_2$ because it is essentially irrelevant to the AFM SFs. Hereafter, safely ignoring $F(\boldsymbol{q})$ to consider the dynamical susceptibility, excluding the specific $\boldsymbol{Q}_1$ and $\boldsymbol{Q}_2$ components, Eq. (1) can be reduced to $(T_1T)^{-1} \approx 2(\gamma_{\mathrm{n}}A_\perp)^2\sum_{\boldsymbol{q}}\frac{\mathrm{Im}\chi_\perp(\boldsymbol{q},\omega_0)}{\omega_0}$ for simplicity.

To decompose each dynamical susceptibility along the i axis in the PM state, a new rate R_i along the quantization i axis can be introduced as $(T_1T)^{-1}_{H_0\|c} = 2R_a$ and $(T_1T)^{-1}_{H_0\|a} = R_c + R_a$. Then, $R_i/(\gamma_{\mathrm{n}}A_i)^2$ corresponds to the dynamical susceptibility divided by ω_0 along the i axis. Figure 7 shows the derived $R_i/(\gamma_nA_i)^2$ vs T ($i = c$ and a) in the PM state under several pressures. Although the pressure and temperature variations of $R_a/(\gamma_nA_a)^2$ exhibit a similar trend, the magnitudes of $R_c/(\gamma_nA_c)^2$ are considerably larger than those of $R_a/(\gamma_nA_a)^2$. In other words, the anisotropy of $R_i/(\gamma_nA_i)^2$ becomes similar to that in $\chi_i(0)$ and K_i at each pressure. As shown in Fig. 7, at ambient pressure, $R_c/(\gamma_nA_c)^2$ is considerably enhanced compared with the a component. When applying pressure, $R_c/(\gamma_nA_c)^2$ is strongly suppressed, and at 0.87 GPa, it shows a broad maximum at approximately $T^*(P) \simeq 50$ K. Near $P_{\mathrm{c}} \simeq 1.08$ GPa, as the temperature decreases below $T^*(P)$, $R_c/(\gamma_nA_c)^2$ decreases monotonically, and then the AFM transition occurs at $T_{\mathrm{N}}(P) = 14$ K. Above P_{c}, as the temperature decreases below T^*, $R_c/(\gamma_nA_c)^2$ decreases and reaches a minimum at approximately ~10 K; then, it slightly increases in the lowest-temperature region. The nearly flat T dependence of $R_i/(\gamma_nA_i)^2$ and K_i below ~10 K and above P_{c} suggests that the Fermi-liquid (FL) state is formed in the T-P region. Indeed, the FL state above P_{c} is detected using thermoelectric power measurements [14].

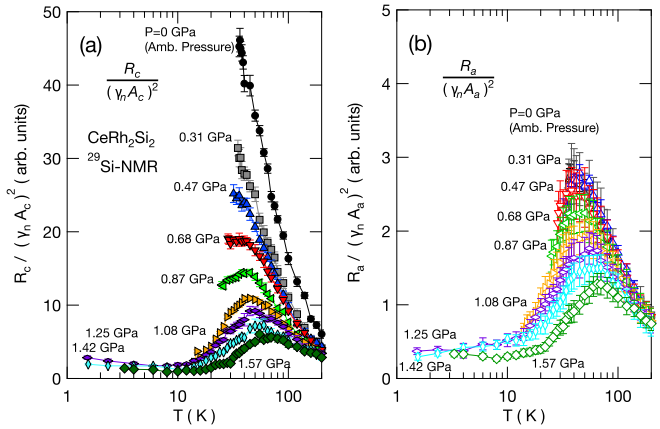

FIG. 7. (a) $R_c/(\gamma_nA_c)^2$ vs T and (b) $R_a/(\gamma_nA_a)^2$ vs T plots for several pressures determined from ^{29}Si NMR relaxation rates in $CeRh_2Si_2$.

In $CeRh_2Si_2$ no critical behavior of $R_c/(\gamma_nA_c)^2$ or $R_a/(\gamma_nA_a)^2$ is observed near P_{c} (Fig. 7), although the AFM transition temperature approaches zero. If the spectral weight of $\mathrm{Im}\chi_i(\boldsymbol{q},\omega_0)$ is again assumed to be centered around $\boldsymbol{Q}$ with $F(\boldsymbol{q}) = 1$, $R_i/(\gamma_nA_i)^2$ would be proportional to $\chi_i(\boldsymbol{Q})/\Gamma_{\boldsymbol{Q},i}$, where $\Gamma_{\boldsymbol{Q},i}$ is a characteristic energy of AFM SFs. If the AFM fluctuations are considerably enhanced, $R_i/(\gamma_nA_i)^2$ should sharply increase because $\chi_i(\boldsymbol{Q})$ increases and $\Gamma_{\boldsymbol{Q},i}$ becomes small. Such a divergent increase in $(T_1T)^{-1}$ is observed in typical HF superconductors, such as $CeIrIn_5$ [28,29], $CeCoIn_5$ [30–32], and $CeRhIn_5$ on the verge of P_{c} [33], the normal states of which are antiferromagnetically enhanced metal. However, in the case of $CeRh_2Si_2$, such enhanced AFM SFs near P_{c} are completely overcome by the hyperfine form factor. Therefore, we cannot determine how the AFM SFs develop under pressure from the $(T_1T)^{-1}$ data. Instead, we can separately clarify the pressure dependence of $\boldsymbol{q}$-independent SFs, i.e., the local fluctuations induced by the Kondo interactions in $CeRh_2Si_2$.

C. Local magnetic fluctuations

At high temperatures at the ambient pressure, at least the dissipation dominantly occurs through local processes by localized Ce moments. In such a case, the dynamical susceptibility can be written in a $\boldsymbol{q}$-independent Lorentzian form:

$$\chi_{\mathrm{L}}(\omega) = \frac{\chi(0)\Gamma_0}{\Gamma_0 - i\omega}, \quad (3)$$

where Γ_0 is the energy scale of the local fluctuations. If the isotropic dynamical susceptibility is assumed, Γ_0 can be obtained as [34–38]

$$\Gamma_0(T) \simeq \left(\gamma_n^2k_{\mathrm{B}}T\right)(T_1)AK/n, \quad (4)$$

where T_1, A, and K are the isotropic components of the NMR relaxation time, hyperfine coupling constant, and NMR shift,

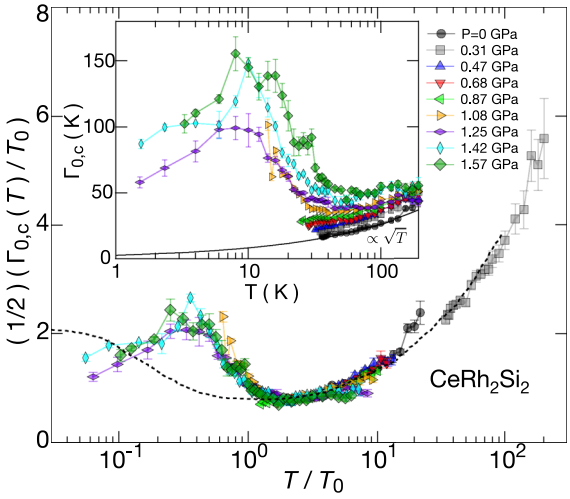

FIG. 8. $\frac{1}{2}\Gamma_{0,c}(T)/T_0$ vs T/T_0 plot for the data in $CeRh_2Si_2$ under various pressures. The dotted curve represents the universal curve calculated for independently screened local moments based on a single Kondo impurity model [39]. The inset shows the temperature dependence of $\Gamma_{0,c}$ at various pressures. The solid curve represents the $\sqrt{T}$ dependence. The legend for the symbols is the same for the inset and main panel.

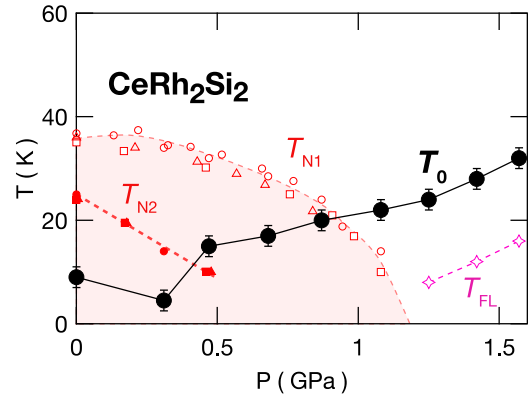

FIG. 9. Pressure dependence of T_0 and T_{FL} in the T-P phase diagram. T_{N1} and T_{N2} (open and solid squares) determined using neutron diffraction in Ref. [23] and resistivity (open and solid triangles) in Ref. [12] are also plotted.

respectively, and n is the number of neighboring magnetic atoms around the observed nucleus. Because the magnetic responses are highly anisotropic in $CeRh_2Si_2$, instead of the isotropic parts, the c components of R_i^{-1}, A_i, and K_i are used in Eq. (4). Thus, $\Gamma_{0,c}(T)$ under pressure is derived as shown in the inset of Fig. 8. The estimated $\Gamma_{0,c}(T)$ at the ambient pressure is consistent with the result obtained from the inelastic neutron scattering experiment [16].

At ambient pressure and $P = 0.31$ GPa, $\Gamma_{0,c}(T)$ follows $\sqrt{T}$ dependence above T_N, as observed in the inset of Fig. 8. Such a $\sqrt{T}$ dependence is considered a characteristic feature of Kondo lattice compounds. When applying pressures of 0.47, 0.68, and 0.87 GPa, $\Gamma_{0,c}(T)$ follows $\sqrt{T}$ dependence in the high-temperature region but slightly deviates upward at low temperatures owing to the formation of Kondo singlets. At 1.08 GPa, $\Gamma_{0,c}(T)$ shows a minimum at approximately 30 K and a steep rise below ~30 K. Above P_c, as the temperature decreases below T_0, $\Gamma_{0,c}(T)$ increases and reaches the maximum at approximately T_{FL} and then decreases below $\sim T_{FL}$.

NMR and neutron scattering experiments [37,38] have indicated that many HF compounds follow the scaling law of $\Gamma_0/T_0 = f(T/T_0)$, which was theoretically calculated by Cox *et al.* for independently screened local moments based on a single Kondo impurity model [39]. The universal curve $f(T/T_0)$ with a single-site Kondo energy scale T_0 can explain the T dependence of Γ_0 in HF materials. Generally, T_0 is proportional to T_K for renormalized high-temperature expansions. In the Kondo lattice compounds, the energy scale will be renormalized by a fixed multiple of T_0. To confirm the single-parameter scaling law, $\frac{1}{2}\Gamma_{0,c}(T)/T_0$ vs T/T_0 is tentatively plotted in Fig. 8. If the energy scale of T_0 is appropriately selected, the system yields a universal curve. Interestingly, the single energy scale of T_0 can describe the respective $\Gamma_{0,c}(T)$. The chosen T_0 at each pressure is shown in Fig. 9. As indicated in this figure, the energy scale of T_0 for local fluctuations shows a monotonic increase in the pressure without a divergent anomaly on the verge of P_c. Consequently, the result agrees with the Doniach picture of the HF phase diagram, where the progressive delocalization of the f electrons occurs with increasing pressure across P_c, along with the development of long-range AFM correlations among the f electrons.

Note that $\frac{1}{2}\Gamma_{0,c}(T)/T_0$ below $P = 1.08$ GPa is always observed in the area of $T/T_0 > 1$, where the f electrons in the system are considered to be localized. At $P = 1.08$ GPa, $\frac{1}{2}\Gamma_{0,c}(T)/T_0$ in the PM state expands in the area below $T/T_0 < 1$; that is, $\Gamma_{0,c}(T)$ starts to increase below T_0, implying that the on-site Kondo screening sets in. At $P = 1.08$ GPa, T_0 becomes approximately 20 K, close to the AFM transition temperature $T_N(P)$, although no critical behavior of Γ_0 or T_0 is observed. Interestingly, the antiferromagnetism suddenly disappears at P_c in the area of $T_N(P) \lesssim T_0$, where the $4f$ moments should be fairly screened by the on-site Kondo interactions. The abrupt disappearance of T_N is also consistent with the abrupt quenching of the ordered moment at 1.08 GPa observed in neutron scattering experiment [23]. The electronic band calculation using the local density approximation + U method [40] suggests that the $4f$ states in the PM state of $CeRh_2Si_2$ located around the Fermi level contribute to the Fermi surface formation, in contrast to the $4f$ orbitals located apart from the Fermi level in the polarized PM state under higher fields and AFM states. In other words, the f electrons in $CeRh_2Si_2$ are barely itinerant at $T = 0$ K.

Last, note that the $(T_1T)^{-1}$ behavior across P_c in $CeRh_2Si_2$ is quite close to that in the prototypical HF antiferromagnet $CeIn_3$. In $CeIn_3$, a similar first-order quantum critical transition at $P_c = 2.46$ GPa, where T_N reaches zero, was revealed using nuclear quadrupole resonance and high-energy x-ray scattering measurements [41]. Furthermore, the pseudogap feature observed in $(T_1T)^{-1}$ in the HF antiferromagnet $CeRhIn_5$ under pressure [42] can also be a signature of $T_0 \sim 4$ K at 1.6 GPa. In $CeRhIn_5$, a sudden change in the Fermi surfaces was observed at $P_c \sim 2.3$ GPa, although the signature of T_0 cannot be resolved in NQR $1/T_1$ near P_c owing to AFM $\chi(\boldsymbol{Q})/\Gamma_{\boldsymbol{Q}}$ enhancement. In the ancestor HF superconductor (S-type) $CeCu_2Si_2$ with no AFM transition, similar Γ_0-T behavior was observed where T_0 was estimated to be ~15 K

[43], while the AFM phase in $CeCu_2Si_2$ introduced by chemical compositional distributions appears to be phase separated [44], indicating the occurrence of a first-order transition. The electronic background in these compounds can be analogous to that in $CeRh_2Si_2$ on the verge of P_c. Thus, the $(T_1T)^{-1}$ behavior across P_c in $CeRh_2Si_2$ exhibits a common feature for the HF antiferromagnets, with the first-order quantum critical transition at P_c. Further theoretical efforts would be required to understand how the superconducting phase is stabilized in such a barely itinerant regime near P_c in which AFM SFs coexist.

IV. SUMMARY

We have performed ^{29}Si NMR experiments on single crystals of the HF antiferromagnet $CeRh_2Si_2$ with ^{29}Si isotopic enrichment of 50%. Because the AFM SFs at specific $\boldsymbol{Q}_1$ and/or $\boldsymbol{Q}_2$ are filtered considerably owing to the hyperfine form factor on the Si sites, the characteristic energy Γ_0 of the $\boldsymbol{q}$-independent fluctuations can be separately estimated using the NMR data in the PM state. The pressure variation of $\Gamma_0(T)$ indicates an incremental increase in the characteristic energy scale T_0 caused by the single-site Kondo effect, which shows no critical divergent behavior around P_c in the HF antiferromagnet $CeRh_2Si_2$. Thus, we microscopically clarified that no Kondo breakdown occurs near P_c in this system and that the progressive delocalization of the f electrons occurs across P_c.

ACKNOWLEDGMENTS

We are grateful for stimulating discussions with K. Kubo, T. Hattori, S. Araki, D. Braithwaite, D. Aoki, H. Ikeda, J. Flouquet, R. E. Walstedt, Z. Fisk, and J. D. Thompson. Part of this work was supported by JSPS KAKENHI Grants No. JP26400341, No. JP17K05522, and No. JP15H05884 and by the REIMEI Research Program of JAEA.

[1] S. Doniach, Phys. B (Amsterdam, Neth.) **91**, 231 (1977).
[2] J. Rossat-Mignod, L. Regnault, J. Jacoud, C. Vettier, P. Lejay, J. Flouquet, E. Walker, D. Jaccard, and A. Amato, J. Magn. Magn. Mater. **76–77**, 376 (1988).
[3] W. Knafo, S. Raymond, P. Lejay, and J. Flouquet, Nat. Phys. **5**, 753 (2009).
[4] Q. Si, S. Rabello, K. Ingersent, and J. L. Smith, Nature (London) **413**, 804 (2001).
[5] P. Gegenwart, Q. Si, and F. Steglich, Nat. Phys. **4**, 186 (2008).
[6] B. H. Grier, J. M. Lawrence, V. Murgai, and R. D. Parks, Phys. Rev. B **29**, 2664 (1984).
[7] S. Kawarazaki, Y. Kobashi, J. A. Fernandez-Baca, S. Murayama, Y. Ōnuki, and Y. Miyako, Phys. B (Amsterdam, Neth.) **206–207**, 298 (1995).
[8] R. Settai, A. Misawa, S. Araki, M. Kosaki, K. Sugiyama, T. Takeuchi, K. Kindo, Y. Haga, E. Yamamoto, and Y. Ōnuki, J. Phys. Soc. Jpn. **66**, 2260 (1997).
[9] S. Araki, A. Misawa, R. Settai, T. Takeuchi, and Y. Ōnuki, J. Phys. Soc. Jpn. **67**, 2915 (1998).
[10] R. Movshovich, T. Graf, D. Mandrus, J. D. Thompson, J. L. Smith, and Z. Fisk, Phys. Rev. B **53**, 8241 (1996).
[11] T. C. Kobayashi, T. Muramatsu, M. Takimoto, K. Hanazono, K. Simizu, K. Amaya, S. Araki, R. Settai, and Y. Ōnuki, Phys. B (Amsterdam, Neth.) **281–282**, 7 (2000).
[12] S. Araki, M. Nakashima, R. Settai, T. C. Kobayashi, and Y. Ōnuki, J. Phys.: Condens. Matter **14**, L377 (2002).
[13] S. Araki, R. Settai, T. C. Kobayashi, H. Harima, and Y. Ōnuki, Phys. Rev. B **64**, 224417 (2001).
[14] A. Palacio Morales, A. Pourret, G. Seyfarth, M. T. Suzuki, D. Braithwaite, G. Knebel, D. Aoki, and J. Flouquet, Phys. Rev. B **91**, 245129 (2015).
[15] A. Villaume, D. Aoki, Y. Haga, G. Knebel, R. Boursier, and J. Flouquet, J. Phys.: Condens. Matter **20**, 015203 (2008).
[16] A. Severing, E. Holland-Moritz, and B. Frick, Phys. Rev. B **39**, 4164 (1989).
[17] T. Willers, D. T. Adroja, B. D. Rainford, Z. Hu, N. Hollmann, P. O. Körner, Y. Y. Chin, D. Schmitz, H. H. Hsieh, H. J. Lin *et al.*, Phys. Rev. B **85**, 035117 (2012).
[18] K. Kitagawa, H. Gotou, T. Yagi, A. Yamada, T. Matsumoto, Y. Uwatoko, and M. Takigawa, J. Phys. Soc. Jpn. **79**, 024001 (2010).
[19] T. Muramatsu, S. Eda, T. C. Kobayashi, M. I. Eremets, K. Amaya, S. Araki, R. Settai, and Y. Ōnuki, Phys. B (Amsterdam, Neth.) **259–261**, 61 (1999).
[20] H. Mori, N. Takeshita, N. Môri, and Y. Uwatoko, Phys. B (Amsterdam, Neth.) **259–261**, 58 (1999).
[21] Y. Kawasaki, K. Ishida, Y. Kitaoka, and K. Asayama, Phys. Rev. B **58**, 8634 (1998).
[22] H. Sakai, Y. Tokunaga, S. Kambe, Y. Matsumoto, T. D. Matsuda, and Y. Haga, J. Korean Phys. Soc. **63**, 352 (2013).
[23] S. Kawarazaki, M. Sato, Y. Miyako, N. Chigusa, K. Watanabe, N. Metoki, Y. Koike, and M. Nishi, Phys. Rev. B **61**, 4167 (2000).
[24] H. Kontani, K. Kanki, and K. Ueda, Phys. Rev. B **59**, 14723 (1999).
[25] R. Boursier, P. Haen, J. Flouquet, Y. Haga, and Y. Ōnuki, Phys. B (Amsterdam, Neth.) **378–380**, 76 (2006).
[26] W. Knafo, D. Aoki, D. Vignolles, B. Vignolle, Y. Klein, C. Jaudet, A. Villaume, C. Proust, and J. Flouquet, Phys. Rev. B **81**, 094403 (2010).
[27] T. Moriya, J. Phys. Soc. Jpn. **18**, 516 (1963).
[28] G.-q. Zheng, K. Tanabe, T. Mito, S. Kawasaki, Y. Kitaoka, D. Aoki, Y. Haga, and Y. Ōnuki, Phys. Rev. Lett. **86**, 4664 (2001).
[29] S. Kambe, H. Sakai, Y. Tokunaga, and R. E. Walstedt, Phys. Rev. B **82**, 144503 (2010).
[30] Y. Kawasaki, S. Kawasaki, M. Yashima, T. Mito, G.-q. Zheng, Y. Kitaoka, H. Shishido, R. Settai, Y. Haga, and Y. Ōnuki, J. Phys. Soc. Jpn. **72**, 2308 (2003).
[31] M. Yashima, S. Kawasaki, Y. Kawasaki, G.-q. Zheng, Y. Kitaoka, H. Shishido, R. Settai, Y. Haga, and Y. Ōnuki, J. Phys. Soc. Jpn. **73**, 2073 (2004).
[32] H. Sakai, S. E. Brown, S. H. Baek, F. Ronning, E. D. Bauer, and J. D. Thompson, Phys. Rev. Lett. **107**, 137001 (2011).
[33] T. Mito, S. Kawasaki, G.-q. Zheng, Y. Kawasaki, K. Ishida, Y. Kitaoka, D. Aoki, Y. Haga, and Y. Ōnuki, Phys. Rev. B **63**, 220507(R) (2001).
[34] A. Narath, CRC Crit. Rev. Solid State Sci. **3**, 1 (1972).

[35] D. E. MacLaughlin, F. R. de Boer, J. Bijvoet, P. F. de Châtel, and W. C. M. Mattens, J. Appl. Phys. **50**, 2094 (1979).
[36] D. E. MacLaughlin, O. Peña, and M. Lysak, Phys. Rev. B **23**, 1039 (1981).
[37] M. Benakki, J. P. Kappler, and P. Panissod, J. Phys. Soc. Jpn. **56**, 3309 (1987).
[38] A. Qachaou, E. Beaurepaire, M. Benakki, B. Lemius, J. Kappler, A. Meyer, and P. Panissod, J. Magn. Magn. Mater. **63–64**, 635 (1987).
[39] D. L. Cox, N. E. Bickers, and J. W. Wilkins, J. Appl. Phys. **57**, 3166 (1985).
[40] A. Pourret, M.-T. Suzuki, A. P. Morales, G. Seyfarth, G. Knebel, D. Aoki, and J. Flouquet, J. Phys. Soc. Jpn. **86**, 084702 (2017).
[41] S. Kawasaki, M. Yashima, Y. Kitaoka, K. Takeda, K. Shimizu, Y. Oishi, M. Takata, T. C. Kobayashi, H. Harima, S. Araki, H. Shishido, R. Settai, and Y. Ōnuki, Phys. Rev. B **77**, 064508 (2008).
[42] S. Kawasaki, T. Mito, Y. Kawasaki, G.-q. Zheng, Y. Kitaoka, D. Aoki, Y. Haga, and Y. Ōnuki, Phys. Rev. Lett. **91**, 137001 (2003).
[43] S. Kitagawa, T. Higuchi, M. Manago, T. Yamanaka, K. Ishida, H. S. Jeevan, and C. Geibel, Phys. Rev. B **96**, 134506 (2017).
[44] K. Ishida, Y. Kawasaki, K. Tabuchi, K. Kashima, Y. Kitaoka, K. Asayama, C. Geibel, and F. Steglich, Phys. Rev. Lett. **82**, 5353 (1999).